ACS Sustainable Chemistry & Engineering

Research Article

pubs.acs.org/journal/ascecg

Organic–Inorganic Composite Films Based on Modified Hemicelluloses with Clay Nanoplatelets

Ying Guan, Bing Zhang, Xin Tan, Xian-Ming Qi, Jing Bian, Feng Peng,* and Run-Cang Sun*

Beijing Key Laboratory of Lignocellulosic Chemistry, Beijing Forestry University, No.35 Tsinghua East Road, Haidian District, Beijing, P. R. China

ABSTRACT: Special challenges and opportunities are present with organic–inorganic composite films with respect to potential applications. The quaternized hemicelluloses (QH) were prepared by etherification of hemicelluloses with ETA under alkaline conditions. The structure of QH was determined by FT-IR and ^{1}H NMR. The biocomposite films were prepared based on QH and montmorillonite (MMT) by a vacuum-filtrated technique. Positively charged QH was paired with exfoliated anionic MMT clay nanoplatelets via electrostatic reaction during the paper-making process. Different ratios of hemicelluloses to clay for the preparation of films were employed. The morphology and structure of the films were characterized by SEM, AFM, FT-IR, and XRD. The thermal properties of the films were explored by thermogravimetric analysis (TGA) and differential scanning calorimetry (DSC), which suggested that the thermal properties were improved by the addition of clay nanoplatelets, whereas the optical transparency of the film decreased with the increment of clay contents. The proper proportion of QH and MMT among the three films was 1:1 based on the results of the thermal and UV–vis transparency properties of films. All of these results suggested that the composite films could be used in areas of application in the coating and packaging fields.

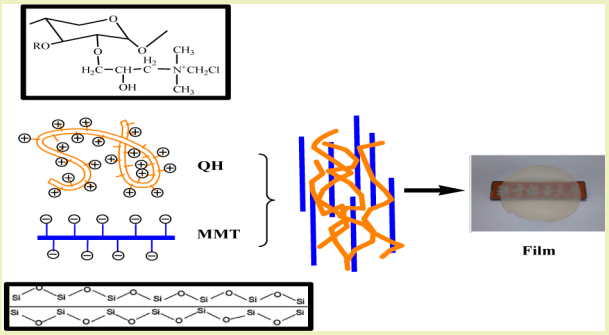

KEYWORDS: *Quaternized hemicelluloses, Montmorillonite, Electrostatic reaction, Composite film*

INTRODUCTION

With the increasing awareness of limited fossil fuels, sustainable sources of materials are urgently needed to supply the needs of society.[1] Nowadays, much attention has been paid to biodegradable materials substituting for nonbiodegradable materials, especially in the application of food packing.[2−4] Among these materials, hemicelluloses, accounting for 20−35% of of lignocellulosic biomass, are the alkali-soluble materials in the plant cell walls, which have been used commercially for production of furfural, xylitol, and wet end additives in paper making.[6] In recent years, increasing interest in hemicelluloses has been rekindled due to their potential film-forming, biodegradable, and biocompatible abilities.[5]

Hemicelluloses can be chemically modified and then transformed into types of functional polymers and useful materials, such as cationic and anionic hemicelluloses, acylated hemicelluloses, and tablet binders.[7−9] The solubility and yields of hemicelluloses were enhanced by the quaternization reaction.[10−12] The quaternized hemicelluloses create various opportunities for obtaining previously unperceived hemicellulose derivatives and functional materials.[13] Some work has been done on hemicellulose-based films, but many problems still exist. Therefore, high value-added utilization of hemicelluloses for packaging and biomedicine are still promising for sustainable industries.

Hybrid nanostructures composed of inorganic nanoplatelets and biomolecules have attracted great interest for applications in nanobiotechnology.[14] The silicate platelets have nanoscale dimensions and possess special properties, such as high intrinsic platelet modulus, strength and ion exchange capability, and large aspect ratio and surface area, as well as high chemical and mechanical stabilities. In addition, the nanoscale silicates could strongly affect the structure and molecular mobility of polymer matrices themselves.[15] Recently, Horrocks and Bourbigot reported that montmorillonite (MMT) clay content (2−5 wt %) in the polymeric materials can strongly reduce their flammability and increase the thermal stability of the materials.[16,17] MMT is made up aluminum silicate layers, and the layers are arranged into stacks in a parallel fashion with regular spacing among them.[18] MMT has very good capability for exfoliating and dispersing in polymer matrices, so it can be employed as a reinforcing agent.[19−22] Therefore, MMT can be used as a filler in many functional polymers, improving the elastic, hydrophobic, and thermoplastic properties of the materials.[23,24] For example, the bioinspired layered composites could be prepared by MMT and other polymers (such as cellulose/poly(vinyl alcohol), poly(*N*-isopropylacrylamide), and graphene oxide), and the composites display impressive strength, which is ordinarily attributed to a compact layered

Received: February 26, 2014
Revised: June 3, 2014
Published: June 17, 2014

   dx.doi.org/10.1021/sc500124j | *ACS Sustainable Chem. Eng.* 2014, 2, 1811−1818

structure, high filler content, and strong inorganic−organic interface.[25−28]

Electrostatic self-assembly is the most used construction mechanism of materials for developing strong, long-range, electrostatic interactions between oppositely charged polyelectrolytes.[29,30] The films, deposited under ambient conditions from water, can be made to exhibit antimicrobial,[31,32] gas barrier,[33−35] electrically conductive,[36,37] flame retardant,[38] and sensing[39] properties by simply exposing a substrate to the mixtures of an opposite charge.[40] Building up the films of polyelectrolyte multilayers through the alternative adsorption of cationic and anionic polyelectrolyte layers is a promising new technique.[41] The electrostatic attraction between oppositely charged polymers is the best known driving force for the formation of multilayered thin films.[42]

In this study, the quaternized hemicelluloses were prepared by the etherification of hemicelluloses and quaternary ammonium salt reagents under alkaline conditions. The structure of modified hemicelluloses was characterized by FT-IR and ^{1}H NMR. A green concept for biopolymer−clay composite films based on QH and MMT nanoplatelets was developed. The strategy was to improve thermal and UV−vis light transparency properties of hemicellulose-based films under moist conditions and rely on nanoelectrostatic interactions. Various films with different proportions of polymer and clay nanoplatelets were investigated by AFM, SEM, FT-IR, XRD, DSC, and optical transparency. This work presents a novel way for assembling this type of film prepared to make hemicellulose substrate flame resistant.

MATERIALS AND METHODS

Materials. Hemicelluloses were exacted by 5% NaOH at 50 °C for 5 h from bamboo (*Phyllostachys pubescens*) holocellulose with a solid to liquid ratio of 1:25 (g mL^{-1}). The holocellulose was obtained by delignification of the dewaxed bamboo (40−60 mesh) with 6% $NaClO_2$ in acidic solution (pH 3.6−3.8) at 75 °C for 2 h. The constituents and molecular weights of the hemicelluloses were determined according to the previous methods.[43] The sugar constituent of the hemicelluloses was 83.6% xylose, 6.8% glucuronic acid, 5.1% arabinose, 4.2% glucose, and 0.4% galactose (relatively molar percent). The molecular weights of hemicelluloses were obtained by gel permeation chromatography and showed that the average molecular weight (M_w) of native hemicelluloses was 13 420 g mol^{-1}. The clay was a montmorillonite (Zhejiang Feng Hong New Material Co., Ltd.). Filter membrane was purchased from Jinteng, Tianjin, China (polyvinylidene fluoride microfiltration membrane, 0.45 μm average pore diameter). 2,3-Epoxypropyltrimethylammonium chloride (ETA) was purchased from Sigma-Aldrich Co., U.S.A. The reagents were analytical reagents.

Preparation of Quaternized Hemicelluloses. The whole reaction process was performed in water media as described in detail by Ren et al.[44] The mixture was stirred at 60 °C, and the total reaction period was 4 h. Upon completion of the reaction, the mixture was cooled to ambient temperature. The reaction mixture was then filtered and washed with ethanol thoroughly. Finally, the sample was obtained by drying in a vacuum oven at 40 °C for 24 h. Degree of quaternization (DQ) was 0.45 by a titration method.[44]

Exfoliation of MMT. A total of 1 wt % MTM (Alfa-Aesar Company) solution was prepared by stirring at 1000 rpm for 30 min and then exfoliating by an ultrasonic processor from Scientz-II D (Ningbo Scientz Biotechnology Co., Ltd). This process was repeated three times, followed by centrifugation of the solution at 3800 rpm for 10 min. The obtained MMT suspension was used for composite preparation.

Preparation of Composite Films. A MMT nanoplatlets solution was mixed with a QH solution of various proportions. The mixed solution was stirred for 12 h and then was vacuum-filtrated with the filter membrane for 20 min. The wet films were carefully peeled off from the membrane after the filtration. Finally, the composite films were dried at ambient temperature. The obtained films with different proportions of QH and MMT were coded as shown in Table 1.

Table 1. Films with Different Proportions in Volumes of QH and MMT

sample codes	V(QH):V(MMT)[a]
F11	1:1
F12	1:2
F21	2:1

[a]Concentrations of QH and MMT were both 2%.

Characterization of Quaternized Hemicelluloses. The FT-IR analysis of QH was recorded on a Thermo Scientific Nicolet iN 10 FT-IR microscope (Thermo Nicolet Corporation, Madison, WI),[45] and the solution-state ^{1}H NMR spectrum of the sample was recorded using a Bruker MSL300 spectrometer (300 MHz) as described by Peng et al.[46]

Film Characterization. The surfaces of films were detected by AFM (Nanoscope III, Veeco) as described elsewhere.[47] SEMs of films were performed with a Hitachi S-3400N II (Hitachi, Japan) instrument as described in a previous study.[45] The crystallinities of the films were measured by a XRD-6000 instrument (Shimadzu, Japan) scanned from 2° to 45° (2θ) with a speed of 5° min^{-1}as described earlier.[48] The thermal properties of film samples recorded by a DTG-60 (Shimadzu, Japan) were described in more detail elsewhere,[49] and the films were heated from 40 to 650 °C at a rate of 20 °C min^{-1}. The DSCs of the films were recorded by a DSC-60 (Shimadzu, Japan) as the method of TGA and were measured at a heating scan rate of 10 °C min^{-1} from the temperature range of 40 to 300 °C. The UV−vis absorption spectra of the samples were determined by an ultraviolet−visible spectrophotometer (Tech comp, UV 2300) in the range of 200−800 nm. The films were pasted on the surface of a quartz pool before UV−vis measurements.

RESULTS AND DISCUSSION

Structural Analysis of Quaternized Hemicelluloses. The FT-IR spectra of hemicelluloses and quaternized hemicelluloses are illustrated in Figure 1. The absorptions at 3411,

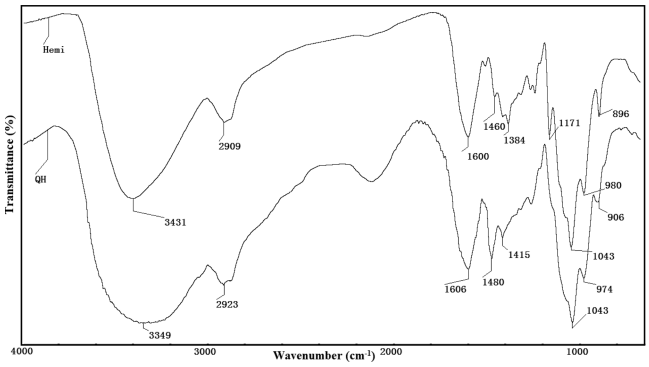

Figure 1. FT-IR spectra of hemicelluloses and modified hemicelluloses.

2909, 1600, 1043, and 896 cm^{-1} are shown in the hemicellulose spectrum. The peaks at about 3411 and 2909 cm^{-1} are indicative of the stretching of the OH groups and C−H vibration band, respectively. The signal at 1600 cm^{-1} is originated from −COO− of the hemicelluloses (uronic acid and uronic carboxylate).[50] The signal at 1043 cm^{-1} is due to the

Scheme 1. Mechanism for Producing the Quaternized Hemicelluloses

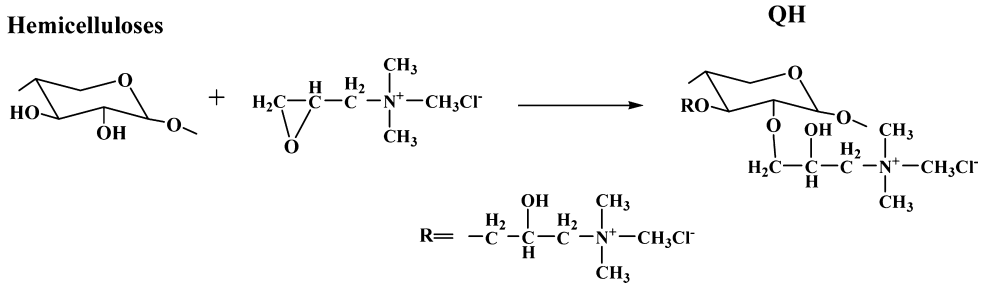

C−O bond stretching frequencies. A sharp band at 896 cm^{-1} is attributed to β-glycosidic linkages between the sugar units.[51] Compared with the spectrum of hemicelluloses, a new band appearing at 1480 cm^{-1} in the spectrum of quaternized hemicelluloses is assigned to the $-CH_3$ groups and methylene bending mode of the quaternized substituent.[52] The signal at 1043 cm^{-1} became broader in the spectrum of the quaternized hemicelluloses compared to that of the peak intensity of native hemicelluloses. These results suggested that the quaternized hemicelluloses were prepared successfully by etherification of hemicelluloses and ETA, introducing the cationic quaternary salt groups into the hemicellulose macromolecules (Scheme 1).

The ^1H NMR spectra of the native hemicelluloses and quaternized hemicelluloses are illustrated in Figure 2. In the spectrum of native hemicelluloses, the peaks from 3.1 to 4.5 ppm are attributed to the protons of anhydroxylose units in the hemicelluloses.[44] An intense signal at 4.7 ppm is assigned to the D_2O. In the spectrum of modified hemicelluloses, the new signals at 4.3 and 4.5 ppm are ascribed to the protons of CH_3 and CH_2 in the quaternary ammonium salt groups.[53] Two peaks at 4.2 ppm, which are attributed to the protons of OH at the C-2 and C-3 positions of the anhydroxylose units, have disappeared. This implied that the substitution of quaternary salt groups occurred at the C-2 and C-3 positions of the anhydroxylose units in the hemicelluloses. These results indicated that the quaternary salt groups were introduced into the hemicellulose macromolecules successfully, which corresponded to the results in FT-IR. When the hemicelluloses have been modified with ETA, which possesses the cationic property, the obtained QH can be used in the preparation of films with anionic MMT by electrostatic interaction.

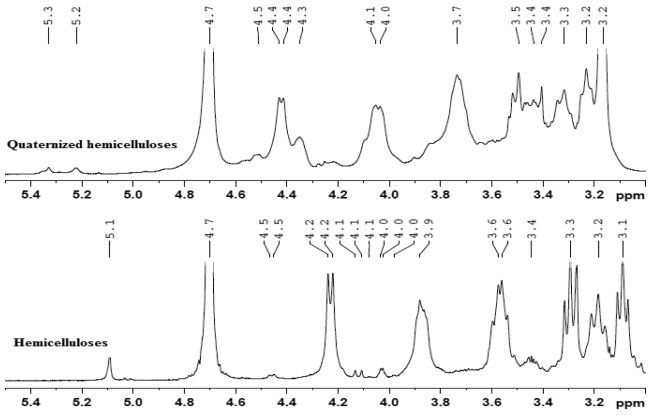

Figure 2. ^1H NMR spectrum of hemicelluloses and modified hemicelluloses.

Morphology of Films. The images of the surface and cross section of the composite film are present in Figure 3. As shown in Figure 3a, the surface of the film is smooth and homogeneous, which indicates that the pattern of the composite film was improved by the introduction of clay nanoplatelets during the electrostatic interaction. In the microstructure of the cross section in Figure 3b, a highly aligned structure indicates that every platelet is laid down on the filter membrane and presented flat. The loading and exfoliation of the clay are formed only by self-assembling during the electrostatic interaction process. MMT clay nanoplatelets were exfoliated to become a negatively charged surface when immersed in water. The aqueous QH has a positive charge. The electrostatic attraction between oppositely charged polymers is the best known driving force for the formation of multilayered thin films (Scheme 2). The nanoplatelet layered structure is formed by the paper-making process, which is very suitable for large-scale manufacturing. The electrostatic and hydrogen-bonding interactions are the primary driving forces for the formation of film multilayers.

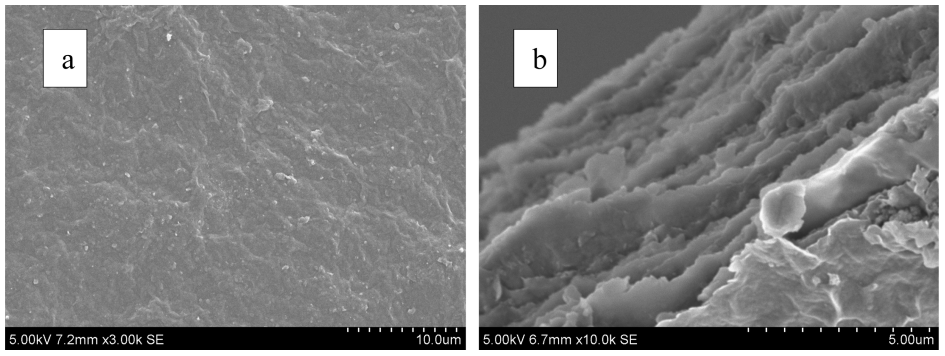

Figure 3. SEM images of the surface (a) and cross section (b) of the composite film.

Scheme 2. Formation Process of Multilayered Thin Films from QH and MMT

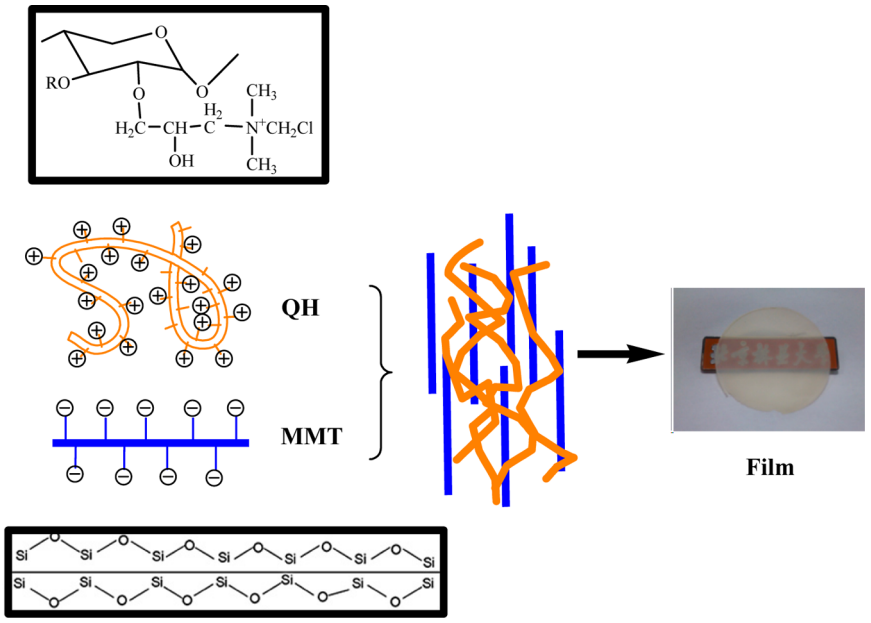

The phase surface images and roughness analyses of F11, F12, and F21 are presented in Figure 4. The AFM phase surface images (Figure 4a,c,e) suggested that the composite films exhibited a relatively complanate surface with few small-size granules, and this phenomenon was in agreement with the SEM images of the films. The MMT platelet was tightly connected with the QH macromolecular chains, forming a rough surface. The roughness values were calculated using 3 μm × 3 μm areas. The roughness of F11, F12, and F21 were 485, 525, and 536 nm, respectively (Figure 4b,d,f), which suggested that the nanoscale film layers were obtained, and the hemicelluloses have been intercalated into the MMT nanoplatelets. The smallest roughness value of F11 among the three films indicated that MMT is deposited densely and formed the complanate surface of the film when the mixture proportion of QH and MMT was 1:1. During the electrostatic interaction process, multilayer films were formed with positively and negatively charged layers by alternating sequential deposition.

Structure of Composite Films. The interaction between QH and MMT was characterized by FT-IR spectroscopy. The FT-IR spectra of QH, MMT, and the nanocomposite films are shown in Figure 5. The signals presented at 1606, 1480, 1043, 974, and 906 cm^{-1} are the characteristic peaks of QH. The bands at 3623 and 1023 cm^{-1} are ascribed to the stretching of Al−OH and Si−O−Si in the MMT spectrum, respectively.[54] The signal at 843 cm^{-1} is attributed to the Al−O−C vibrational band of MMT.[55] In the spectrum of the film, the frequency of the vibrational band at 3623 cm^{-1} is assigned to the Al−OH stretching band of MMT, and the peak at 3349 cm^{-1} corresponded to the hydrogen-bonding of QH. A signal at 843 cm^{-1} originated from the vibration of MMT, indicating that the Al−QH bonds were formed through the OH group of the QH interacting with Al on the MMT surface.[56] Although this peak is weak, it is still representative of the occurrence of the molecular interaction between QH and MMT. This result suggested that no chemical reaction happened between MMT and QH and that QH was intercalated into the MMT nanoplatelets.

X-ray diffraction analysis was carried out to determine the dispersion of the MMT layers in the matrix of the hemicelluloses. The XRD patterns of MMT, QH, and the QH−MMT composite film are shown in Figure 6a. It is well known that pristine MMT exhibited an amorphous X-ray diffraction pattern over Bragg angles of 3−9°, as reported in the literature.[57,58] A characteristic peak of MMT was detected at 7.4° in the XRD pattern of MMT (Figure 6a). In the pattern of hemicelluloses, only one broad peak is shown at 21.6°. The diffraction peaks were shifted to 18.7° and 24.3° in the diffraction of the composite film, indicating that the intercalated hybrid structures were produced by electrostatic reaction. The diffraction peaks of the film were shifted to higher angles, which was due to a change in the crystal plane.[59,60] In other words, the deviation of angles was related to the decrease in the constant and volume of the crystal lattice, and then the crystal plane was changed. It was mainly due to the fact that QH was intercalated into the MMT nanoplatelets, and the new crystal plane was formed during this process.

The effects of the polymer content on the peak intensities are shown in Figure 6b. The characteristic peaks of the composite films with different polymer proportions exhibited different intensities from the three patterns. As the amount of QH in the matrix of the film composites was increased, the intensities of the peaks become low. The diffraction intensity of the films was reduced by adding the noncrystalline QH, and the lowest intensity of the two characteristic peaks was present at the XRD pattern of F21 with the highest content of the QH among the three composite films. Therefore, the proper proportions of QH and MMT were the most important factors in the preparation of films.

Thermal Properties of Films. To investigate the thermal properties of the composite films, the TGAs of MMT, QH, and the composite films were studied. The TGA curves of MMT, QH, and the composite films are illustrated in Figure 7. The weight loss below 100 °C was mainly due to the moisture release of the samples. From the TGA curve of MMT, there is still 91.45% residue mass of MMT when the temperature reached 650 °C, which indicated that MMT has a relative high

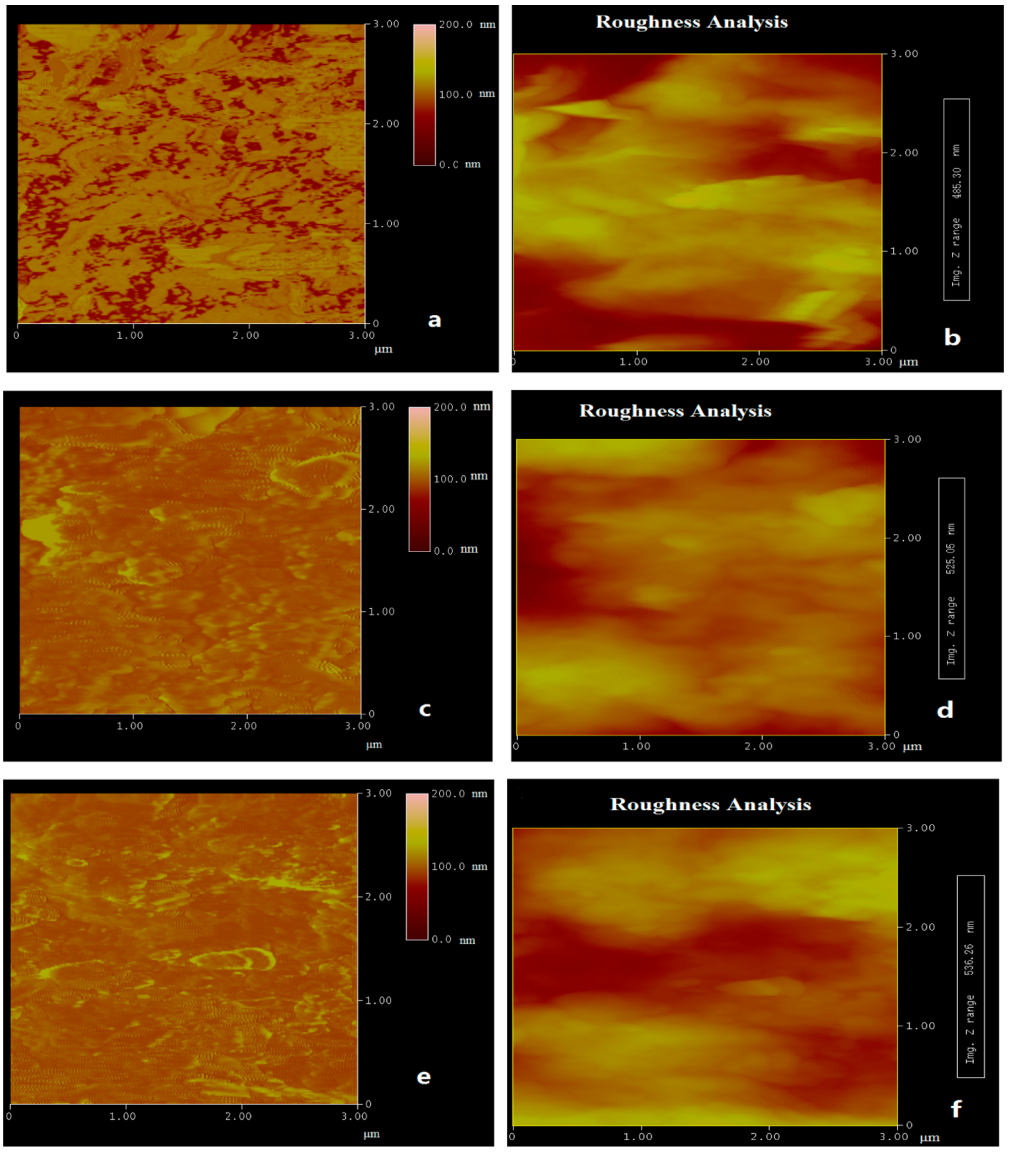

Figure 4. AFM phase surface image (a,c,e) and roughness analysis (b,d,f) of F11, F12, and F21.

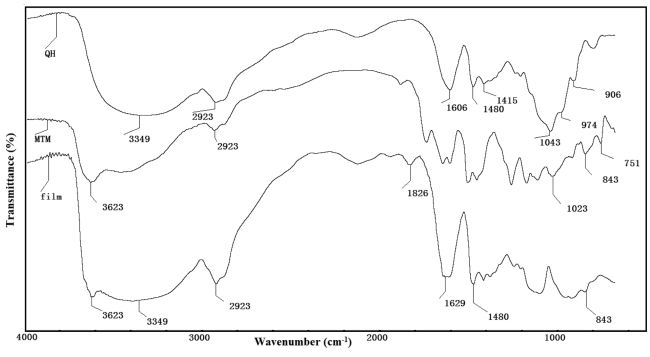

Figure 5. FT-IR spectra of QH, MMT, and the composite film.

thermal stability. This could contribute to the flame retardant property of the composite film for the package applications. Obviously, the thermal stabilities of the three films were higher than those of QH, which was due to the addition of MMT. Meanwhile, the thermal stabilities of these films increased with the increment of MMT content in the order of F12 > F11 > F21. In addition, DSC was carried out to determine the thermal characteristic of the three film samples. The DSC curves of the composite films with different proportions of QH and MMT are investigated in Figure 8. The endothermic peaks of the three composite films were all around 270 °C, which suggested that the composite film possessed a high thermal stability. This peak has been mainly corresponded to the melting of the crystalline MMT during retrogradation. The melting temperature of the films increased from 262.8 to 272.1 °C when the MMT contents increased from 2:1 to 1:2 in the proportion of QH and MMT. The changes in this peak indicated that the MMT contents form the crystal domains and decrease the movement of the hemicellulose chains. The glass transition in the three curves was not present, which suggested that QH was fully intercalated into the MMT nanoplatelets, and this favored a well-ordered arrangement of QH and MMT. A photograph of the film after combustion is shown in Figure 8a. The shape of the film was unchanged after the combustion, indicating that the composite film possessed good thermal stability with the MMT as the platelet.

UV−Vis Transparency of Films. The UV−vis spectra of the three film samples are shown in Figure 9. The

dx.doi.org/10.1021/sc500124j | ACS Sustainable Chem. Eng. 2014, 2, 1811−1818

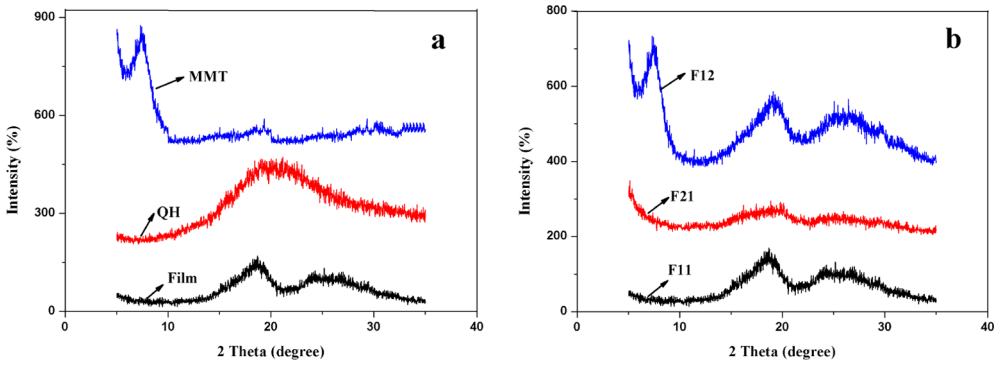

Figure 6. (a) XRD of QH, MMT, and composite film. (b) XRD of F11, F12, and F21 (b).

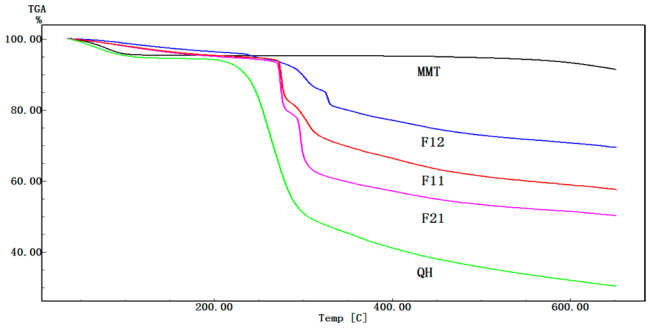

Figure 7. TGA curves of MMT, QH, F11, F12, and F21.

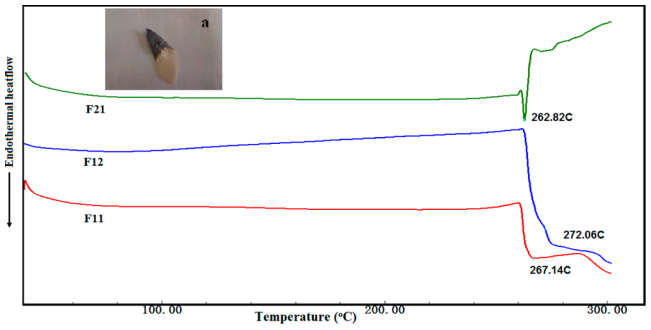

Figure 8. DSC thermogram of the composite films with different proportions of QH and MMT.

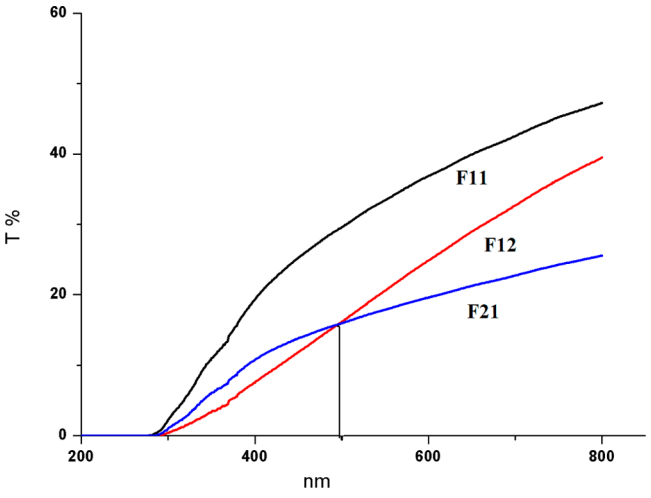

Figure 9. UV−vis spectra of composite films with different proportions of QH and MMT.

transparencies of all composite films increase from the UV light to visible light. The three films exhibit transmittance in the UV and visible ranges, which are a favorable effect for food protection. When the proportion of QH and MMT was 1:1, the UV and visible light transparency of the film was the highest. It was confirmed that the proper proportion of QH and MMT among the three samples was 1:1, which corresponded to the result of DSC. Compared to F12 and F21, the transparency of F21 was higher than that of F12 at the UV range and lower than that of F12 above 500 nm. The exact reason for this phenomenon is not completely known, but the results indicate that the transparencies of F12 and F 21 are lower than that of F11.

CONCLUSIONS

Cationic hemicelluloses were prepared successfully by quaternization with ETA and hemicelluloses. The analyses of FT-IR and ^{1}H NMR indicated that the cationic quaternary salt groups were introduced into the hemicellulose macromolecules. Flat, heat-resisting, hemicellulose-based hybrid films were prepared with montmorillonite platelets as the inorganic phase by a water-based paper-making procedure. The nanoscale film layers were obtained, and the film surface was smooth and homogeneous. The thermal properties of the composite films were improved by the addition of clay nanoplatelets, and the transparency of F11 (the proportion of QH and MMT was 1:1) was higher than that of the others. It was found that the QH intercalated into the MMT nanoplatelets by electrostatic and hydrogen-bonding interactions, and the proper proportion of QH and MMT among the composite films was 1:1. These results suggested that nanocomposite films are of great interest for use as a flame retardant in packaging applications.

AUTHOR INFORMATION

Corresponding Authors

*E-mail: fengpeng@bjfu.edu.cn. Tel./Fax: +86-10-62336972 (F.P.).

*E-mail: rcsun3@bjfu.edu.cn. Tel./Fax: +86-10-62336972 (R.-C.S.).

Notes

The authors declare no competing financial interest.

ACKNOWLEDGMENTS

This work was supported by the Fundamental Research Funds for the Central Universities (BLYJ201416), Beijing Higher Education Young Elite Teacher Project (YETP0764), Ministries of Education (NCET-13-0670, 113014A), Ministry of

Science and Technology (973 project, 2010CB732204), and National Science and Technology Program of the Twelfth Five-Year Plan Period (2012BAD32B06).

REFERENCES

(1) Ragauskas, A. J.; Williams, C. K.; Davison, B. H.; Britovsek, G.; Cairney, J.; Eckert, C. A.; Frederick, W. J.; Hallett, J. P.; Leak, D. J.; Liotta, C. L.; Mielenz, J. R.; Murphy, R.; Templer, R.; Tschaplinski, T. The path forward for biofuels and biomaterials. *Science* **2006**, *311*, 484−489.

(2) Ghasemlou, M.; Khodaiyan, F.; Oromiehie, A.; Yarmand, M. S. Development and characterisation of a new biodegradable edible film made from kefiran, an exopolysaccharide obtained from kefir grains. *Food Chem.* **2011**, *127*, 1496−1502.

(3) Xiong, H. G.; Tang, S. W.; Tang, H. L.; Zou, P. The structure and properties of a starch-based biodegradable film. *Carbohydr. Polym.* **2008**, *71*, 263−268.

(4) Alves, V. D.; Costa, N.; Coelhoso, I. M. Barrier properties of biodegradable composite films based on kappa-carrageenan/pectin blends and mica flakes. *Carbohydr. Polym.* **2010**, *79*, 269−276.

(5) Sun, R.-C.; Sun, X. F.; Tomkinson, J. Hemicelluloses and Their Derivatives. In *Hemicellulose: Science and Technology*; Gatenholm, P., Tenkanen, M., Eds.; ACS Symposium Series 864; American Chemical Society: Washington, DC, 2004, pp 2−22.

(6) Timell, T. E. Recent progress in the chemistry of wood hemicelluloses. *Wood Sci. Technol.* **1967**, *l*, 45−70.

(7) Ren, J. L.; Sun, R.-C.; Liu, C. F.; Lin, L.; He, B. H. Synthesis and characterization of novel cationic SCB hemicelluloses with a low degree of substitution. *Carbohydr. Polym.* **2007**, *67*, 347−357.

(8) Schwikal, K.; Heinze, T.; Ebringerova, A.; Petzold, K. Cationic xylan derivatives with high degree of functionalization. *Macromol. Symp.* **2006**, *232*, 49−56.

(9) Petzold, K.; Schwikal, K.; Günther, W.; Heinze, T. Carboxymethyl Xylan-Control of Properties by Synthesis. *Macromol. Symp.* **2006**, *232*, 27−36.

(10) Haack, V.; Heinze, T.; Oelmeyer, G.; Kulicke, W. M. Starch derivatives of high degree of functionalization, 8. Synthesis and flocculation behavior of cationic starch polyelectrolytes. *Macromol. Mater. Eng.* **2002**, *287*, 495−502.

(11) Zhang, L. M. Preparation and anti-clay-swelling ability of new water soluble cellulose derivatives containing quaternary ammonium groups. *J. Appl. Polym. Sci.* **2001**, *79*, 1416−1422.

(12) Thanou, M. M.; Kotzé, A. F.; Scharringhausen, T.; Lueβen, H. L.; de Boer, A. G.; Verhoef, J. C. Effect of degree of quaternization of *N*-trimethyl chitosan chloride for enhanced transport of hydrophilic compounds across intestinal Caco-2 cell monolayers. *J. Controlled Release* **2000**, *64*, 15−25.

(13) Peng, X. W.; Ren, J. L.; Sun, R.-C. An efficient method for the synthesis of hemicellulosic derivatives with bifunctional groups in butanol/water medium and their rheological properties. *Carbohydr. Polym.* **2011**, *83*, 1922−1928.

(14) Niemeyer, C. M. Nanoparticles, proteins, and nucleic acids: Biotechnology meets materials science. *Angew. Chem., Int. Ed.* **2001**, *40*, 4128−4158.

(15) Százdi, L.; Pozsgay, A.; Pukánszky, B. Factors and processes influencing the reinforcing effect of layered silicates in polymer nanocomposites. *Eur. Polym. J.* **2007**, *43*, 345−373.

(16) Horrocks, A. R.; Kandola, B. K.; Smart, G.; Zhang, S.; Hull, T. R. Polypropylene fibers containing Dispersed clays having improved fire performance. I. Effect of nanoclays on processing parameters and fiber properties. *J. Appl. Polym. Sci.* **2007**, *106*, 1707−1717.

(17) Bourbigot, S.; Devaux, E.; Flambard, X. Flammability of polyamide-6/clay hybrid nanocomposite textiles. *Polym. Degrad. Stab.* **2002**, *75*, 397−402.

(18) Moucka, R.; Mravcakova, M.; Vilcakova; Omastova, J. M.; Saha, P. Electromagnetic absorption efficiency of polypropylene/montmorillonite/polypyrrole nanocomposites. *Mater. Design.* **2011**, *32*, 2006−2011.

(19) Khatana, S.; Dhibar, A. K.; Ray, S. S.; Khatua, B. B. Use of pristine clay platelets as a suspension stabilizer for the synthesis of poly(methyl methacrylate)/clay nanocomposites. *Macromol. Chem. Phys.* **2009**, *210*, 1104−1113.

(20) Lin, R. Y.; Chen, B. S.; Chen, G. L.; Wu, J. Y.; Chiu, H. C.; Suen, S. Y. Preparation of porous PMMA/Na^+−montmorillonite cation-exchange membranes for cationic dye adsorption. *J. Membr. Sci.* **2009**, *326*, 117−129.

(21) Oral, A.; Tasdelen, M. A.; Demirel, A. L.; Yagci, Y. Poly(methyl methacrylate)/clay nanocomposites by photoinitiated free radical polymerization using intercalated monomer. *Polymer* **2009**, *50*, 3905−3910.

(22) Wu, T. F.; Xie, T. X.; Yang, G. S. Preparation and characterization of transparent poly(methyl methacrylate)/Na +-MMT nanocomposite films by solution casting. *J. Appl. Polym. Sci.* **2010**, *115*, 2773−2778.

(23) Jain, R. K.; Sjostedt, M.; Glasser, W. Thermoplastic xylan derivatives with propylene oxide. *Cellulose* **2000**, *7*, 319−336.

(24) Lima, D. U.; Oliveira, R. C.; Buckeridge, M. S. Seed storage hemicelluloses as wet-end additives in papermaking. *Carbohydr. Polym.* **2003**, *52*, 367−373.

(25) Wang, J. F.; Lin, L.; Cheng, Q. F.; Jiang, L. A strong bio-inspired layered PNIPAM-clay nanocomposite hydrogel. *Angew. Chem., Int. Ed.* **2012**, *51*, 4676−4680.

(26) Wang, J. F.; Cheng, Q. F.; Lin, L.; Jiang, L. Synergistic toughening of bioinspired poly(vinyl alcohol)-clay-nanofibrillar cellulose artificial nacre. *ACS Nano* **2014**, *8*, 2739−2745.

(27) Cheng, Q. F.; Wu, M. X.; Li, M. Z.; Jiang, L.; Tang, Z. Y. Ultratough artificial nacre based on conjugated cross-linked graphene oxide. *Angew. Chem., Int. Ed.* **2013**, *52*, 3750−3755.

(28) Cheng, Q. F.; Jiang, L.; Tang, Z. Y. Bioinspired layered materials with superior mechanical performance. *Acc. Chem. Res.* **2014**, *47*, 1256−1266.

(29) Decher, G.; Hong, J. D.; Schmitt, J. Buildup of ultrathin multilayer films by a self-assembly process: III. Consecutively alternating adsorption of anionic and cationic polyelectrolytes on charged surfaces. *Thin Solid Films* **1992**, *210−211*, 831−835.

(30) Costa, R. R.; Testera, A. M.; Javier Arias, F.; Carlos Rodríguez-Cabello, J.; Mano, J. F. Layer-by-Layer film growth using polysaccharides and recombinant polypeptides: A combinatorial approach. *J. Phys. Chem. B* **2013**, *117*, 6839−6848.

(31) Dvoracek, C. M.; Sukhonosova, G.; Benedik, M. J.; Grunlan, J. C. Antimicrobial behavior of polyelectrolyte-surfactant thin film assemblies. *Langmuir* **2009**, *25*, 10322−10328.

(32) Boulmedais, F.; Frisch, B.; Etienne, O.; Lavalle, P.; Picart, C.; Ogier, J.; Voegel, J. C.; Schaaf, P.; Egles, C. Polyelectrolyte multilayer films with pegylated polypeptides as a new type of anti-microbial protection for biomaterials. *Biomaterials* **2004**, *25*, 2003−2011.

(33) Jang, W. S.; Rawson, I.; Grunlan, J. C. Layer-by-layer assembly of thin film oxygen barrier. *Thin Solid Films* **2008**, *516*, 4819−4825.

(34) Priolo, M. A.; Gamboa, D.; Holder, K. M.; Grunlan, J. C. Super gas barrier of transparent polymer-clay multilayer ultrathin films. *Nano Lett.* **2010**, *10*, 4970−4974.

(35) Svagan, A. J.; Akesson, A.; Cardenas, M.; Bulut, S.; Knudsen, J. C.; Risbo, J.; Plackett, D. Transparent films based on PLA and montmorillonite with tunable oxygen barrier properties. *Biomacromolecules* **2012**, *13*, 397−405.

(36) Park, Y. T.; Ham, A. Y.; Yang, Y. H.; Grunlan, J. C. Fully organic ITO replacement through acid doping of double-walled carbon nanotube thin film assemblies. *RSC Adv.* **2011**, *1*, 662−671.

(37) Vosgueritchian, M.; Lipomi, D. J.; Bao, Z. A. Highly conductive and transparent PEDOT: PSS films with a fluorosurfactant for stretchable and flexible transparent electrodes. *Adv. Funct. Mater.* **2012**, *22*, 421−428.

(38) Li, Y. C.; Mannen, S.; Morgan, A. B.; Chang, S. C.; Yang, Y. H.; Condon, B.; Grunlan, J. C. Intumescent all-polymer multilayer nanocoating capable of extinguishing flame on fabric. *Adv. Mater.* **2011**, *23*, 3926−3931.

(39) Liu, S.; Yan, J.; He, G.; Zhong, D.; Chen, J.; Shi, L.; Zhou, X.; Jiang, H. Layer-by-layer assembled multilayer films of reduced graphene oxide/gold nanoparticles for the electrochemical detection of dopamine. *J. Electro. Anal. Chem.* **2012**, *672*, 40−44.
(40) Holder, K. M.; Priolo, M. A.; Secrist, K. E.; Greenlee, S. M.; Nolte, A. J.; Grunlan, J. C. Humidity-responsive gas barrier of hydrogen-bonded polymer-clay multilayer thin films. *J. Phys. Chem. C* **2012**, *116*, 19851−19856.
(41) Decher, G. Fuzzy nanoassemblies: Toward layered polymeric multicomposites. *Science* **1997**, *277*, 1232−1237.
(42) Dammak, A.; Moreau, C.; Beury, N.; Schwikal, K.; Winter, H. T.; Bonnin, E.; Saake, B.; Cathala, B. Elaboration of multilayered thin films based on cellulose nanocrystals and cationic xylans: Application to xylanase activity detection. *Holzforschung* **2013**, *67*, 579−586.
(43) Peng, F.; Ren, J. L.; Xu, F.; Bian, J.; Peng, P.; Sun, R.-C. Comparative study of hemicelluloses obtained by graded ethanol precipitation from sugarcane bagasse. *J. Agr. Food Chem.* **2009**, *57*, 6305−6317.
(44) Ren, J. L.; Peng, F.; Sun, R.-C. Preparation of hemicellulosic derivatives with bifunctional groups in different media. *J. Agric. Food Chem.* **2008**, *56*, 11209−11216.
(45) Guan, Y.; Bian, J.; Peng, F.; Zhang, X. M.; Sun, R.-C. High strength of hemicelluloses based hydrogels by freeze/thawtechnique. *Carbohydr. Polym.* **2014**, *101*, 272−280.
(46) Peng, F.; Bian, J.; Peng, P.; Guan, Y.; Xu, F.; Sun, R.-C. Fractional separation and structural features of hemicelluloses from sweet sorghum leaves. *BioResources* **2012**, *7*, 4744−4759.
(47) Peng, X. W.; Ren, J. L.; Zhong, L. X.; Sun, R.-C. Nanocomposite films based on xylan-rich hemicelluloses and cellulose nanofibers with enhanced mechanical properties. *Biomacromolecules* **2011**, *12*, 3321−3329.
(48) Guan, Y.; Zhang, B.; Bian, J.; Peng, F.; Sun, R.-C. Nanoreinforced hemicellulose-based hydrogels prepared by freeze−thaw treatment. *Cellulose* **2014**, *21*, 1709−1721.
(49) Xiao, L. P.; Shi, Z. J.; Bai, Y. Y.; Wang, W.; Zhang, X. M.; Sun, R.-C. Biodegradation of lignocellulose by white-rot fungi: structural characterization of water-soluble hemicelluloses. *Bioenerg. Res.* **2013**, *6*, 1154−1164.
(50) Kačuráková, M.; Wellner, N.; Ebringerová, A.; Hromádková, Z.; Wilson, R. H.; Belton, P. S. Characterisation of xylan-type polysaccharides and associated cell wall components by FT-IR and FT-Raman spectroscopies. *Food Hydrocolloid.* **1999**, *13*, 35−41.
(51) Ebringerová, A.; Hromádková, Z.; Alföldi, J.; Berth, G. Structural and solution properties of corn cob eteroxylans. *Carbohydr. Polym.* **1992**, *19*, 99−105.
(52) Kačuráková, M.; Ebringerová, A.; Hirsch, J.; Hromádková, Z. Infrared study of arabinoxylans. *J. Agr. Food Chem.* **1994**, *66*, 423−427.
(53) Ren, J. L.; Peng, F.; Sun, R.-C.; Liu, C. F.; Cao, Z. N.; Luo, W.; Tang, J. N. Synthesis of cationic hemicellulosic derivatives with a low degree of substitution in dimethyl sulfoxide media. *J. Appl. Polym. Sci.* **2008**, *109*, 2711−2717.
(54) Liu, M. X.; Li, W. D.; Rong, J. H.; Zhou, C. R. Novel polymer nanocomposite hydrogel with natural clay nanotubes. *Colloid Polym. Sci.* **2012**, *290*, 895−905.
(55) Liu, A. D.; Walther, A.; Ikkala, O.; Belova, L.; Berglund, L. A. Clay nanopaper with tough cellulose nanofiber matrix for fire retardancy and gas barrier functions. *Biomacromolecules* **2011**, *12*, 633−641.
(56) Liang, C. Y.; Marchessault, R. H. J. Infrared spectra of crystalline polysaccharides. II. Native celluloses in the region from 640 to 1700 cm^{-1}. *Polym. Sci.* **1959**, *37*, 385−395.
(57) Barber, G. D.; Calhoun, B. H.; Moore, R. B. Poly(ethylene terephthalate) ionomer based clay nanocomposites produced via melt extrusion. *Polymer* **2005**, *46*, 6706−6714.
(58) Zhu, J.; Wang, X.; Tao, F.; Xue, G.; Chen, T.; Sun, P.; Jin, Q.; Ding, D. Room temperature spontaneous exfoliation of organo-clay in liquid polybutadiene: Effect of polymer end-groups and the alkyl tail number of organic modifier. *Polymer* **2007**, *48*, 7590−7597.
(59) Tezcan, F.; Günister, E.; Özen, G.; Erim, F. B. Biocomposite films based on alginate and organically modified clay. *Int. J. Biol. Macromol.* **2012**, *50*, 1165−1168.
(60) Almasi, H.; Ghanbarzadeh, B.; Entezami, A. A. Physicochemical properties of starch-CMC-nanoclay biodegradable films. *Int. J. Biol. Macromol.* **2010**, *46*, 1−5.